ACADEMIC PRESS

Available online at www.sciencedirect.com

SCIENCE DIRECT®

Journal of Computational Physics 185 (2003) 252–270

JOURNAL OF COMPUTATIONAL PHYSICS

www.elsevier.com/locate/jcp

A Laplace transform/potential-theoretic method for acoustic propagation in subsonic flows☆

S.I. Hariharan [a,*], Scott Sawyer [b], D. Dane Quinn [b]

[a] *Department of Electrical and Computer Engineering and Division of Applied Mathematics, The University of Akron, Akron, OH 44325-3904, USA*

[b] *Department of Mechanical Engineering, Akron, OH 44325-3903, USA*

Received 22 February 2002; received in revised form 27 September 2002; accepted 18 November 2002

Abstract

This paper introduces a competitive computational approach for determining time-dependent far-field sound generated by subsonic flows around lifting airfoils. The procedure assumes the linearity of the sound field away from a bounded region surrounding the airfoil. It is assumed that the sound pressure on the boundary of this enclosed region (referred to as the Kirchhoff surface) is specified, possibly by another procedure such as solving the full Euler equations. Away from the Kirchhoff surface, the Euler equations are linearized about a uniform mean flow. It is well known that linearized Euler equations can be uncoupled into a scalar convective wave equation. However, due to the anisotropy present in the convective wave equation, it is difficult to compute solutions. In this context, direct numerical simulation of the convective wave equation requires proper numerical descriptions of far-field boundary conditions which is a non-trivial task. Moreover, if accurate far-field conditions can be formulated, the computational cost of direct simulation can be prohibitive even in a modest computational domain. In this paper, we present an alternate solution procedure. First, the problem is transformed via the Laplace transform (with appropriate initial conditions) into a reduced wave equation. The convective term in the reduced wave equation is removed using a dependent variable transformation. Then we use Gothert's rule, to obtain a Helmholtz like equation with complex wave number, which is subsequently solved using double layer potential theory. Finally upon application of numerical inverse Laplace transform techniques, far-field acoustic pressure is obtained as a function of space and time.

Keywords: Potential theory; Computational aeroacoustics; Laplace transforms

1. Introduction

The prediction of far-field sound radiation has received a considerable amount of attention in the computational aeroacoustics community and commonly arises in unsteady external aerodynamic problems

☆ Supported by a grant from NASA Glenn Research Center, Grant No. NAG3-2182 and by NSF Grant ANI-981807.
* Corresponding author.
E-mail addresses: hari@uakron.edu (S.I. Hariharan), ssawyer@uakron.edu (S. Sawyer), quinn@uakron.edu (D. Dane Quinn).

0021-9991/02/$ - see front matter
doi:10.1016/S0021-9991(02)00056-6

such as the gust response of airfoils, flutter problems, and jet noise. These problems are commonly posed in open domains where it is difficult to extend the computational domain to the far field due to the dissipative and dispersive properties of direct numerical schemes. Thus, several researchers have attacked open domain problems by splitting the domain into acoustic near- and far-fields. The near-field which is typically nonlinear may be calculated using a variety of computational techniques available to date. In the far-field, the linear nature dominates, and, in particular, the linearized Euler equations with constant coefficients accurately represent the flow field.

A sequence of works developed by Atassi and his coworkers [1–3,5,6] exploit this linear behavior in the far-field and couple this procedure to the interior numerical scheme. They employ frequency domain numerical simulations (limited to a single frequency harmonic) in the near-field [7,8], and determine the far-field sound using Kirchhoff techniques. Thus, the driving philosophy of this work is to provide an accurate near-field numerical simulation coupled with a ''semi-analytical'' approach to predict the far-field sound. The work of Atassi et al. [2,3,5,6] uses a Kirchhoff method and modified Green's function approach wherein Kirchhoff's formula is used to predict the far-field sound. In their work, because of numerical difficulties in calculating the normal pressure derivative on the Kirchhoff surface a modified, approximate Green's function was used.

In contrast, the potential-theoretic method is implemented in [18,19] using a single layer potential method which requires only the free space Green's function and an unknown single layer density. The application of this method for determining the far-field acoustics of an airfoil which is subject to an upstream harmonic gust was discussed in [18] and [19] in detail. This single layer density is determined using a technique proposed by Hariharan and MacCamy [4] for electromagnetic scattering problems using a singular integral equation of the first kind. In this paper, we use double layer potentials, so that a well-posed second kind integral equation is obtained. The potential-theoretic methods, whether they be single layer or double layer, have the following advantages:

- Far-field radiation conditions are built in the formulation.
- Unlike other Kirchhoff formulations, potential-theoretic methods do not call for normal derivatives of pressure on a Kirchhoff surface.
- These methods are easy to implement. Singularities resulting from the formulation are analytically removed.
- Results compare extremely well with semi-analytical and other proven results for radiation of sound produced by flows around thin airfoils ([18,19]).
- The general geometry of the Kirchhoff surface is not limited to a circle or a sphere as in other Kirchhoff models.

In this paper, we combine the application of Laplace transforms with results from potential theory to develop a fast and accurate procedure, referred to as the transform potential-theoretic (TPT) technique, for the determination of the time-dependent far-field propagation of sound. The complete solution procedure is as follows: (a) determine the acoustic near-field around the airfoil using a non-reflecting boundary condition [20]; (b) extract the pressure on an artificial boundary, called 'the Kirchhoff surface' in the paper; and (c) then solve the problem in the exterior using the TPT technique. It is assumed that the near-field up to the Kirchhoff surface, governed by the Euler equations, is obtained using an appropriate solution technique with accurate radiation boundary conditions. Away from this surface, the field equations can linearized and reduced to the convective wave equation. We use the Laplace transform and Gothert's rule to reduce the convective wave equation to the Helmholtz equation, where initial conditions are properly chosen and dictated by the physics of the problem. Then, the solution of the problem is sought by the application of potential theory. We specifically use a double layer potential to describe a fast and efficient procedure. The double layer potential has the advantage that the resulting kernel function is non-singular. Moreover, the double layer potential method allows for higher order numerical quadrature rules in the resulting integral equations. Finally, we invert the transformed solutions to time domain using the techniques proposed in

[16]. The procedure described in this paper combines the Laplace transform, potential theory and the inverse Laplace transform to determine the time-dependent far-field acoustic pressure. The results obtained through the TPT are compared to the direct numerical simulations with accurate high order boundary conditions procedure developed by Hagstrom and Hariharan [21]. Sample calculations are presented to demonstrate the accuracy and the computational efficiency of the TPT technique.

The use of transform methods such as the Laplace transforms advocated here to study time-dependent wave motions in electromagnetics have been investigated in the context of finite element solutions in the past [9]. Numerical inversion associated with this type of techniques have been investigated extensively in the literature [11–14]. For the far field calculations, use of Kirchhoff's methods are nicely summarized in [28]. In particular, for the three-dimensional problem, exact time-domain formulation is given. In contrast, we consider a two-dimensional case for which this formulation is not possible due to the absence of Huygen's principle. In a sequence of works by [23–25], the authors demonstrate highly accurate boundary conditions based on the work by Hagstrom and Hariharan [20] in conjunction with the direct simulation of far field radiation. Also in the paper by Alpert et al. [27], the authors have provided a novel procedure for rapid evaluation of non-reflecting boundary kernels for time-dependent wave equations. This work provides a competitive approach for evaluating exact boundary conditions with less work than that is required for the local formulation, such as the one proposed in [20]. Use of this method still requires direct simulation and is costly due to the fact that direct methods require large number of nodes to extend the solution to the far field. These authors also provided an integral evolution formula for the wave equation in [26]. While this method looks promising, no details are yet available for far field calculations.

2. General formulation

The general class of problem that is of interest is modeled after an airfoil gust interaction model. For this purpose, we consider an upstream gust that interacts with an airfoil which is in a uniform subsonic flow at infinity. We construct a Kirchhoff surface which surrounds the flow region in the near-field. The surface will be referred to as Γ and the exterior of the surface as Ω. For now, our only assumption is that Γ is smooth and is far enough away from the airfoil so that the mean flow quantities in Ω differ only very slightly from the free stream. This allows us to linearize the continuity and momentum equations about the freestream flow using

$$\boldsymbol{U} = \boldsymbol{U}_\infty + \hat{\boldsymbol{u}}, \tag{1}$$

$$\rho = \rho_\infty + \hat{\rho}, \tag{2}$$

$$p = p_\infty + \hat{p}, \tag{3}$$

where ∞ subscripts indicate freestream quantities. These decompositions lead to the linearized continuity and momentum equations in Ω:

$$\frac{D_\infty \hat{\rho}}{Dt} + \rho_\infty \nabla \cdot \hat{\boldsymbol{u}} = 0, \tag{4}$$

$$\rho_\infty \frac{D_\infty \hat{\boldsymbol{u}}}{Dt} + \nabla \hat{p} = 0, \tag{5}$$

where $D_\infty/Dt \equiv \partial/\partial t + U_\infty \cdot \partial/\partial x$. Taking D_∞/Dt of Eq. (4) and applying the *div* operator to Eq. (5) gives

$$\frac{D_\infty^2 \hat{\rho}}{Dt^2} + \rho_\infty \frac{D_\infty}{Dt}(\nabla \cdot \hat{\boldsymbol{u}}) = 0, \tag{6}$$

$$\rho_\infty \frac{D_\infty}{Dt}(\nabla \cdot \hat{\boldsymbol{u}}) + \nabla^2 \hat{p} = 0. \tag{7}$$

To eliminate $\hat{\boldsymbol{u}}$ from the above equations, we subtract Eq. (7) from Eq. (6) and obtain

$$\frac{D_\infty^2 \hat{\rho}}{Dt^2} = \nabla^2 \hat{p}. \tag{8}$$

The state equations relating p and ρ are

$$p = A\rho^\gamma, \quad \frac{\partial p}{\partial \rho} = c_\infty^2 \qquad (\gamma = 1.4 \text{ for standard air}), \tag{9}$$

where A is a constant. Combining these with the linearizations in Eqs. (2) and (3) gives the relation

$$\hat{p} = c_\infty^2 \hat{\rho}. \tag{10}$$

Substituting Eq. (10) into Eq. (8) gives

$$\frac{1}{c_\infty^2}\frac{D_\infty^2 \hat{p}}{Dt^2} = \nabla^2 \hat{p}, \tag{11}$$

which reduces the problem to one dependent variable only, namely $\hat{p}$. After non-dimensionalizing appropriately the linearized continuity and momentum equations reduce to

$$\left(\frac{\partial}{\partial t} + M_\infty \frac{\partial}{\partial x}\right)^2 \hat{p} = \nabla^2 \hat{p}. \tag{12}$$

3. Problem statement

From this point, all quantities are assumed to be non-dimensional. To setup the problem, we begin with Eq. (12)

$$\left(\frac{\partial}{\partial t} + M_\infty \frac{\partial}{\partial x}\right)^2 \hat{p} = \nabla^2 \hat{p} \quad \text{in } \Omega, \tag{13}$$

where Ω is the unbounded domain exterior to the Kirchhoff surface Γ. We restrict our attention to two-dimensional acoustic disturbances $\hat{p} = \hat{p}(x, y, t)$. On the Kirchhoff surface Γ,

$$\hat{p}(x, y, t) = \hat{f}(x, y, t). \tag{14}$$

The initial conditions are

$$\hat{p}(x, y, 0) = 0,$$
$$\hat{p}_t(x, y, 0) = 0.$$

In addition $\hat{p}(x, y, t)$ satisfies the raditation condition as $r = \sqrt{x^2 + y^2} \to \infty$.

Now we convert the problem to the transformed domain by taking the Laplace transform of Eq. (12). This yields

$$\left(s + M_\infty \frac{\partial}{\partial x}\right)^2 \tilde{p} = \nabla^2 \tilde{p}, \tag{15}$$

where $\tilde{p}(x,y,s)$ is the Laplace transform of $\hat{p}(x,y,t)$. Now, this equation can be further reduced via the transformation

$$\tilde{p} = e^{\lambda x}\bar{p} \quad \text{with } \lambda = \frac{M_\infty s}{1 - M_\infty^2}. \tag{16}$$

Finally scaling x and y as

$$x = (1 - M_\infty^2)\bar{x}, \quad y = \sqrt{1 - M_\infty^2}\,\bar{y}, \tag{17}$$

the reduced wave equation becomes

$$\nabla^2 \bar{p} = s^2 \bar{p}. \tag{18}$$

This is a Helmholtz equation with imaginary wave number $k = \mathrm{i}s$, for which potential theory (simple or double layer potentials) applies. It should be noted that Green's function now has to be evaluated using complex arguments. This is easily accomplished by the formulas found in [22]. Thus in essence, the problem can be solved for each fixed s, the independent variable introduced by the Laplace transform. To realize these results in the time domain, as mentioned before, we borrow results known in the electrical engineering literature. Note that in this transformation process the Kirchhoff surface Γ is transformed to $\bar{\Gamma}$, and the exterior domain Ω is transformed to $\bar{\Omega}$ (see [18]). After application of the Laplace transform and the transformation of the dependent variable, the pressure on the Kirchhoff surface $\hat{f}(x,y,t)$ becomes $\bar{f}(\bar{x},\bar{y},s) = \tilde{f}(x,y,s)e^{-\lambda x}$.

4. Double layer potentials

Now given the Kirchhoff surface $\bar{\Gamma}$ and the evaluated pressure in the frequency domain from an interior solver on this surface, interpolated from another code such as an Euler Solver, one can use a double layer potential to determine the far-field acoustic pressure in the frequency domain. Given the pressure $\bar{p} = \bar{f}$ on the Kirchhoff surface $\bar{\Gamma}$ (see Fig. 1)

$$\bar{p}(\bar{\boldsymbol{x}}) = \int_{\bar{\Gamma}} \bar{\mu}(\bar{\boldsymbol{\xi}}) \frac{\partial G_{\mathrm{f}}(\bar{\boldsymbol{x}} \,|\, \bar{\boldsymbol{\xi}})}{\partial n_{\bar{\boldsymbol{\xi}}}} \, \mathrm{d}s_{\bar{\xi}}, \quad \bar{\boldsymbol{x}} \in \bar{\Omega}, \ \ \bar{\boldsymbol{\xi}} \in \bar{\Gamma}, \tag{19}$$

where G_{f} is the free space Green's function given by

$$G_{\mathrm{f}}(\bar{\boldsymbol{x}} \,|\, \bar{\boldsymbol{\xi}}) = -\frac{\mathrm{i}}{4} H_0^{(1)}(k|\bar{\boldsymbol{x}} - \bar{\boldsymbol{\xi}}|) \quad \text{with } k = \mathrm{i}s. \tag{20}$$

Moreover, $\bar{p}$ satisfies the radiation condition

$$\bar{p} \sim \frac{e^{\mathrm{i}kR}}{\sqrt{R}} \ \text{ as } |\bar{\boldsymbol{x}}| \to \infty \quad \text{with } R = |\bar{\boldsymbol{x}} - \bar{\boldsymbol{\xi}}|, \tag{21}$$

while $\bar{p} = \bar{f}(\bar{\boldsymbol{x}})$ on the boundary $\bar{\Gamma}$. In the expression for the double layer potential, the quantity $\bar{\mu}(\bar{\boldsymbol{x}})$ represents the potential density associated with the value of the pressure on the Kirchhoff surface.

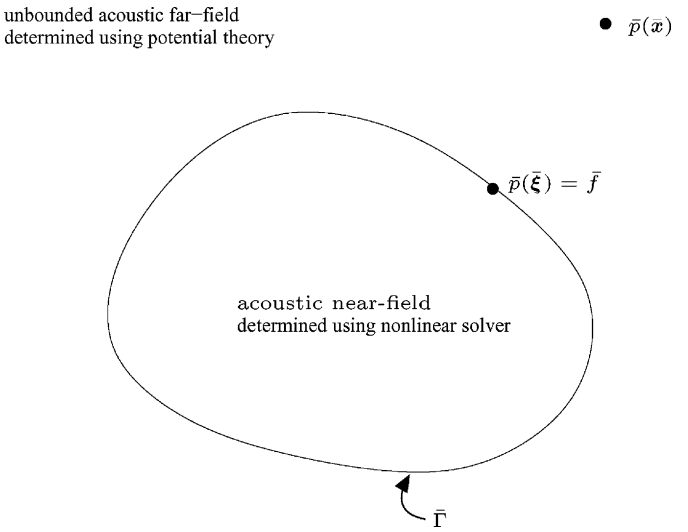

Fig. 1. The far-field pressure can be determined given the pressure on $\bar{\Gamma}$.

On the boundary $\bar{\Gamma}$, the double layer potential can be represented as an integral equation of the second kind

$$-\frac{1}{2}\bar{\mu}(\bar{\boldsymbol{x}}) + \int_{\bar{\Gamma}} \bar{\mu}(\bar{\boldsymbol{\xi}}) \frac{\partial G_{\mathrm{f}}(\bar{\boldsymbol{x}} \mid \bar{\boldsymbol{\xi}})}{\partial n_{\bar{\xi}}} \, \mathrm{d}s_{\bar{\xi}} = \bar{f}(\bar{\boldsymbol{x}}), \quad \bar{\boldsymbol{x}}, \bar{\boldsymbol{\xi}} \in \bar{\Gamma}. \tag{22}$$

Upon parameterization with arc-length variable $\bar{\boldsymbol{x}} = \bar{\boldsymbol{x}}(l)$, we find that the integral equation reduces to

$$-\frac{1}{2}\bar{\mu}(l) + \int_0^L \mathscr{K}(l,\tau)\bar{\mu}(\tau)\,\mathrm{d}\tau = \bar{f}(l), \quad 0 \leqslant l < L, \tag{23}$$

where $\bar{\mu}(l) \equiv \bar{\mu}(\bar{\boldsymbol{x}}(l))$, $\bar{f}(l) \equiv \bar{f}(\bar{\boldsymbol{x}}(l))$, and

$$\mathscr{K}(l,\tau) = -\frac{\mathrm{i}}{4} k H_0^{(1)'}(kd(l,\tau)) \; \frac{-\bar{y}'(\tau)\Big(\bar{x}(l) - \bar{x}(\tau)\Big) + \bar{x}'(\tau)\Big(\bar{y}(l) - \bar{y}(\tau)\Big)}{d(l,\tau)}. \tag{24}$$

In this expression $d(l,\tau)$ is the Euclidean distance between $\bar{\boldsymbol{x}}(l)$ and $\bar{\boldsymbol{x}}(\tau)$, that is,

$$d(l,\tau) = \sqrt{\Big(\bar{x}(l) - \bar{x}(\tau)\Big)^2 + \Big(\bar{y}(l) - \bar{y}(\tau)\Big)^2}.$$

In contrast to the simple layer potential, the kernel in this equation has no singularity. Near the origin the Hankel function has a logarithmic singularity, so that as $\bar{\boldsymbol{x}}$ approaches $\bar{\boldsymbol{\xi}}$ along the Kirchhoff surface, using local Taylor expansions in Eq. (24), one can show

$$\lim_{l \to \tau} \mathscr{K}(l,\tau) = \frac{\kappa(l)}{4\pi}, \tag{25}$$

where κ is the curvature of the boundary given by

$$\kappa(l) = \bar{x}'(l)\bar{y}''(l) - \bar{y}'(l)\bar{x}''(l).$$

Computationally, it is more convenient to work with a polar representation of the domain. Representing the Kirchhoff surface by $\bar{r} = \bar{r}(\bar{\theta})$, assuming the boundary is convex shaped, we have

$$(\bar{x}(l(\bar{\theta})), \bar{y}(l(\bar{\theta}))) = (\bar{r}(\bar{\theta})\cos\bar{\theta}, \bar{r}(\bar{\theta})\sin\bar{\theta}),$$
$$(\bar{x}(l(\bar{\phi})), \bar{y}(l(\bar{\phi}))) = (\bar{r}(\bar{\phi})\cos\bar{\phi}, \bar{r}(\bar{\phi})\sin\bar{\phi}).$$

We identify $J = \sqrt{(\bar{r})^2 + (\bar{r}')^2}$ as the dilation factor and

$$d(\bar{\theta}, \bar{\phi}) = \sqrt{\bar{r}^2(\bar{\theta}) - 2\bar{r}(\bar{\theta})\bar{r}(\bar{\phi})\cos(\bar{\theta} - \bar{\phi}) + \bar{r}^2(\bar{\phi})}.$$

With the use of polar coordinates, the kernel becomes

$$\mathscr{K}(\bar{\theta}, \bar{\phi}) = \frac{ik}{4} H_1^{(1)}(kd(\bar{\theta}, \bar{\phi})) \frac{\bar{G}(\bar{\theta}, \bar{\phi})}{d(\bar{\theta}, \bar{\phi})}, \tag{26}$$

where

$$\bar{G}(\theta, \phi) = \frac{\bar{r}(\bar{\theta})\bar{r}'(\bar{\phi})\sin(\bar{\theta} - \bar{\phi}) - \bar{r}(\bar{\theta})\bar{r}(\bar{\phi})\cos(\bar{\theta} - \bar{\phi}) + \bar{r}^2(\bar{\phi})}{J(\bar{\phi})},$$

and when $\bar{\theta} = \bar{\phi}$, the kernel reduces to

$$\mathscr{K}(\bar{\theta}, \bar{\theta}) = \frac{1}{4\pi} \frac{\left(\bar{r}^2(\bar{\theta}) - 2\bar{r}(\bar{\theta})\bar{r}'(\bar{\theta})\sin 2\bar{\theta} + 2\bar{r}'^2(\bar{\theta})\cos(2\bar{\theta}) - \bar{r}(\bar{\theta})\bar{r}''(\bar{\theta})\right)}{J^3(\bar{\theta})}.$$

Therefore, the integral equation that determines the potential density on the boundary, Eq. (23), becomes

$$-\frac{1}{2}\bar{\mu}(\bar{\theta}) + \int_0^{2\pi} \mathscr{K}(\bar{\theta}, \bar{\phi}) J(\bar{\phi})\, \bar{\mu}(\bar{\phi})\, \mathrm{d}\bar{\phi} = \bar{f}(\bar{\theta}), \quad 0 \leqslant \bar{\theta} < 2\pi. \tag{27}$$

5. Numerical considerations

Solution of the above-described problem entails solving Eq. (27), an integral equation of the second kind, to determine $\bar{\mu}(\bar{\boldsymbol{y}})$ for $\bar{\boldsymbol{y}} \in \bar{\Gamma}$. We solve the integral equation, Eq. (27), by a rectangular quadrature rule. To do so we divide the angular variables into n_θ equal intervals as follows:

$$\bar{\theta}_i = (i-1)h, \quad i = 1, 2, \ldots, n_\theta,$$
$$\bar{\phi}_j = (j-1)h, \quad j = 1, 2, \ldots, n_\theta,$$

with $h = 2\pi/n_\theta$. Then the discrete form of Eq. (27) becomes

$$-\frac{1}{2}\bar{\mu}_i + h\sum_{j=1}^{n_\theta} \mathscr{K}(\bar{\theta}_i, \bar{\phi}_j) J(\bar{\phi}_j) \bar{\mu}_j = \bar{f}(\bar{\theta}_i),$$

or compactly

$$\left[-\frac{1}{2}\boldsymbol{I} + h\boldsymbol{K}\right]\bar{\boldsymbol{\mu}} = \bar{\boldsymbol{f}}\ ,$$

where

$$K_{ij} = \mathcal{K}(\bar{\theta}_i, \bar{\phi}_j) J(\bar{\phi}_j), \quad \bar{\mu}_i = \bar{\mu}(\bar{\theta}_i), \quad \bar{f}_i = \bar{f}(\bar{\theta}_i).$$

This algebraic system can be solved by several computational techniques. Formally

$$\bar{\boldsymbol{\mu}} = \left[-\frac{1}{2}\boldsymbol{I} + h\boldsymbol{K} \right]^{-1} \bar{\boldsymbol{f}} \ .$$

Once $\bar{\boldsymbol{\mu}}(\bar{\xi}, s)$ is known, the pressure $\bar{p}(\bar{\boldsymbol{x}}, s)$ throughout the region $\bar{\boldsymbol{x}} \in \Omega$ may be determined from Eq. (19). To calculate $p(\bar{\boldsymbol{x}}, t)$, this is followed by a Laplace inversion, and an inversion of the transformation described in Eqs. (16) and (17).

6. Time-domain inversion techniques

Let $f(t)$ be a real function of t, with $f(t) = 0$ for $t < 0$; the Laplace transform pair is defined as follows:

$$F(s) = \int_0^\infty \mathrm{e}^{-st} f(t)\,\mathrm{d}t, \quad s = a + \mathrm{i}\omega, \tag{28}$$

$$f(t) = \frac{1}{2\pi\mathrm{i}} \int_{a-\mathrm{i}\infty}^{a+\mathrm{i}\infty} \mathrm{e}^{st} F(s)\,\mathrm{d}s, \tag{29}$$

where a is arbitrary, but is greater than the real parts of all singularities of the image function $F(s)$. Generally speaking, we want to reconstruct a time-dependent function $f(\boldsymbol{x}, t)$ from its image $\hat{F}(\boldsymbol{x}, s)$, where $\boldsymbol{x}$ denotes the spatial dependence. For any physical system, if there exists no exponentially growing component, all the poles should locate at the left half (including the imaginary axis) of the s-plane. Thus, in the following discussion, we assume that $a > 0$. Even when the image function is given in analytical form, the direct evaluation of Eq. (29) is extremely difficult (except for those that can be found in the Laplace transform tables). Therefore, we pursue a numerical procedure. While there are several different methods available [10], the Fourier series method is well-established, due to the methods to determine "optimal" parameters, given in [16].

We begin with a discussion on the trigonometric integral representation of the inversion formula. Eq. (28) can be expanded into

$$\begin{aligned} F(s) &= \int_0^\infty \mathrm{e}^{-at} f(t) \cos\omega t\,\mathrm{d}t - \mathrm{i}\int_0^\infty \mathrm{e}^{-at} f(t) \sin\omega t\,\mathrm{d}t, \\ &= \Re\{F(a+\mathrm{i}\omega)\} + \mathrm{i}\Im\{F(a+\mathrm{i}\omega)\}, \end{aligned}$$

where $s = a + \mathrm{i}\omega$. In turn, Eq. (29) is expanded into

$$\begin{aligned} f(t) = {} & \frac{\mathrm{e}^{at}}{2\pi} \int_{-\infty}^{\infty} (\Re\{F(a+\mathrm{i}\omega)\} \cos\omega t - \Im\{F(a+\mathrm{i}\omega)\} \sin\omega t)\,\mathrm{d}\omega \\ & + \mathrm{i}\frac{\mathrm{e}^{at}}{2\pi} \int_{-\infty}^{\infty} (\Im\{F(a+\mathrm{i}\omega)\} \cos\omega t + \Re\{F(a+\mathrm{i}\omega)\} \sin\omega t)\,\mathrm{d}\omega. \end{aligned} \tag{30}$$

From Eq. (28), we see that $F(\bar{s}) = \overline{F(s)}$, because $f(t)$ is a real function. This condition is equivalent to

$$\Re\{F(a-\mathrm{i}\omega)\} + \mathrm{i}\Im\{F(a-i\omega)\} = \Re\{F(a+\mathrm{i}\omega)\} - \mathrm{i}\Im\{F(a+i\omega)\}.$$

Thus, $\Re\{F(a+\mathrm{i}\omega)\}$ is even and $\Im\{F(a+\mathrm{i}\omega)\}$ is an odd function of ω. This allows one to reduce the infinite integral to a semi-infinite representation

$$f(t) = \frac{\mathrm{e}^{at}}{\pi}\int_0^\infty (\Re\{F(a+\mathrm{i}\omega)\}\cos\omega t - \Im\{F(a+\mathrm{i}\omega)\}\sin\omega t)\,\mathrm{d}\omega. \tag{31}$$

The Fourier series approximation of Eq. (31), presented by Dubner and Abate [15], is obtained by right Riemann sums, and is given by

$$f(t) \simeq \frac{\mathrm{e}^{at}}{T}\left[-\frac{1}{2}\Re\{F(a)\} + \sum_{k=0}^{\infty}\Re\left\{F\left(a+\frac{k\pi\mathrm{i}}{T}\right)\right\}\cos\left(\frac{k\pi t}{T}\right) - \sum_{k=0}^{\infty}\Im\left\{F\left(a+\frac{k\pi\mathrm{i}}{T}\right)\right\}\sin\left(\frac{k\pi t}{T}\right)\right] \tag{32}$$

with a discretization error

$$E_{\mathrm{D}}(a,t,T) = \sum_{n=1}^{\infty}\mathrm{e}^{-2nTa}[f(2nT+t)]. \tag{33}$$

As the infinite series given in Eq. (32) can only be summed up to N terms, there occurs a truncation error

$$E_{\mathrm{T}}(N,a,t,T) = \frac{\mathrm{e}^{at}}{T}\left[\sum_{k=N+1}^{\infty}\Re\left\{F\left(a+\frac{k\pi\mathrm{i}}{T}\right)\right\}\cos\left(\frac{k\pi t}{T}\right) - \sum_{k=N+1}^{\infty}\Im\left\{F\left(a+\frac{k\pi\mathrm{i}}{T}\right)\right\}\sin\left(\frac{k\pi t}{T}\right)\right]. \tag{34}$$

Finally, the approximate value of $f(t)$ is

$$f(t) \simeq \frac{\mathrm{e}^{at}}{T}\left[-\frac{1}{2}\Re\{F(a)\} + \sum_{k=0}^{N}\Re\left\{F\left(a+\frac{k\pi\mathrm{i}}{T}\right)\right\}\cos\left(\frac{k\pi t}{T}\right) - \sum_{k=0}^{N}\Im\left\{F\left(a+\frac{k\pi\mathrm{i}}{T}\right)\right\}\sin\left(\frac{k\pi t}{T}\right)\right]. \tag{35}$$

The accuracy of Eq. (35) depends on the choice of the free parameters (N,a,T). The essence of this method is that one can reduce the errors for any fixed (N,T) by choosing $a>0$ appropriately. Honig and Hirdes [16] have presented two definitions for such an "optimal" a. For any fixed (N,T), the parameter a is optimal if (A) the absolute values of the discretization error, Eq. (33) and the truncation error Eq. (34) are equal; and (B) the sum of the absolute values of the discretization and truncation error is minimal.

We first consider case (A). One can write the truncation error E_{T} in the form

$$E_{\mathrm{T}}(N,a,t,T) = \frac{\mathrm{e}^{at}}{T}R(N),$$

where

$$R(N) = \sum_{k=N+1}^{\infty}\Re\left\{F\left(a+\frac{k\pi\mathrm{i}}{T}\right)\right\}\cos\left(\frac{k\pi t}{T}\right) - \Im\left\{F\left(a+\frac{k\pi\mathrm{i}}{T}\right)\right\}\sin\left(\frac{k\pi t}{T}\right).$$

The approximate value for $f(t)$ is

$$f_N(t) \simeq f(t) - \frac{\mathrm{e}^{at}}{T}R(N) + \mathrm{O}(\mathrm{e}^{-2aT}).$$

To calculate $R(N)$, we choose two parameters a_1 and a_2 large, with $a_1 \neq a_2$. Then

$$f_N^1(t) - f_N^2(t) \simeq \frac{R(N)}{T}(\mathrm{e}^{a_2 t} - \mathrm{e}^{a_1 t}),$$

or

$$R(N) \simeq T\frac{f_N^1(t) - f_N^2(t)}{\mathrm{e}^{a_2 t} - \mathrm{e}^{a_1 t}}.$$

Also write the discretization error E_{D} in the form

$$E_{\mathrm{D}}(a,t,T) = \mathrm{e}^{-2aT} f(2T+t) + \mathrm{O}(\mathrm{e}^{-4aT}),$$

and we find

$$a_{\mathrm{opt}}^i \simeq -\frac{1}{2T+t}\ln\left|\frac{R(N)}{Tf_N(2T+t)}\right|.$$

Now consider case (B), which requires that

$$\frac{\partial}{\partial a}\left[\frac{\mathrm{e}^{at}}{T}|R(N,a)| + |E_{\mathrm{D}}(a,t,T)|\right]_{a=a_{\mathrm{opt}}^B} = 0.$$

This can be evaluated by an iterative procedure

$$\frac{\partial|R(N,a^{(i)})|}{\partial a} \simeq \frac{R(N,a^{(i-1)}) - R(N,a_1^{(i-1)})}{a^{(i-1)} - a_1^{(i-1)}}, \quad i = 1,\ldots,n,$$

$$a^{(0)} = a_{\mathrm{opt}}^A,\ \ a_1^{(0)} = a_1,\ \ a_1^{(i)} = a^{(i-1)}, \quad i = 1,\ldots,n,$$

$$a^{(i)} = -\frac{1}{2T+t}\ln\left[\frac{\frac{\partial|R(N,a^{(i)})|}{\partial a} + |R(N,a^{(i)})|t}{2T^2|f_N(2T+t)|}\right], \quad i = 1,\ldots,n,$$

$$a_{\mathrm{opt}}^B = a^{(n)}.$$

One obvious advantage in this formulation is that s-values are known before the numerical inversion is performed. This is very important when a closed form solution is not available for the physical problem of interest. The numerical methods have to be adopted to solve differential or integral equations and the s-values are given by

$$s_k = a + \frac{k\pi\mathrm{i}}{T}, \quad k = 0,\ldots,N.$$

The above method has been successfully used to reconstruct time-dependent functions $f(t)$, including the step function, from the associated close-formed image functions [15]. Toward applications, [17] reported results to one- and two-dimensional transient heat conduction problems in which finite-difference and finite element methods were invoked to solve transformed differential equations, but the authors did not provide guidance to choose optimal parameters when the unknown function is spatially dependent. We fill this gap with the ideas indicated above and extend the applications to CAA problems.

In summary, we have developed a solution procedure for the time-domain far-field sound propagation, based on potential theory and using the Laplace transform and its inverse. We believe this is a powerful method and an attractive alternative to the conventional CAA methods. The possible applications are

numerous. The method incorporates arbitrary geometries of the Kirchhoff surfaces and in this aspect is ideal for jet noise problems, in which the computational domains are typically narrow and long. Further, it has exact far-field behavior built-in. As a result, it avoids challenging issues such as accurate absorbing boundary conditions and their complex implementations, etc. Finally, the formulations can be extended to three dimensions, though much work and ideas are still needed.

7. Numerical Laplace transform

The first step in the solution procedure is the determination of the Laplace transform of the boundary data which are provided at discrete time intervals Δt over the time period $T = N_{\Delta t}\Delta t$, where $N_{\Delta t}$ is the number of samples. Thus, the Laplace transform given in Eq. (28) must be evaluated numerically at the frequencies of interest. With boundary data given as a discrete function of time

$$f(r_m, \theta_l, t) \approx f(r_m, \theta_l, t_j),$$

where $t_j = j\Delta t$, the Laplace transform

$$F(\theta_l, s) = \int_0^\infty \mathrm{e}^{-st} f(\theta_l, t)\,\mathrm{d}t,$$

is integrated numerically using Simpson's 1/3 with an even number of panels and $N_{\Delta t}$ odd, so that

$$F(\theta_l, s_k) \approx \frac{T}{3N_{\Delta t}}\left(f(\theta_l, t_0) + 4\sum_{j=1,3,5}^{N_{\Delta t}-1} \mathrm{e}^{-s_k t_j} f(\theta_l, t_j) + 2\sum_{j=2,4,6}^{N_{\Delta t}-2} \mathrm{e}^{-s_k t_j} f(\theta_l, t_j) + f(\theta_l, t_{N_{\Delta t}}) \right),$$

where $s_k = a + \mathrm{i}(k\pi/T)$. The approximation will hold given an adequately small time interval and if, for $j > N_{\Delta t}$, $f(\theta_l, t_j) \approx 0$. As outlined above, the optimum value of a is determined through an iterative procedure. For each iteration, a new value of a is determined, and the Laplace transform must be recalculated from the original time series.

8. Results

In this section, the effectiveness of the TPT technique will be demonstrated for a two-dimensional far-field acoustic radiation problem. The acoustic pressure is specified on a circular boundary that through the application of the transformations described in Section 2 becomes an ellipse. Interior to this ellipse the acoustic field must be determined using an appropriate linear or nonlinear direct numerical simulation that is beyond the scope of this paper. The purpose of this research is to demonstrate that given the acoustic pressure on the specified boundary, the ensuing far-field sound can be efficiently calculated in the unbounded exterior domain. The most common alternative solution procedure is the recalculation or extension of the direct numerical simulation, which can be prohibitive in terms of computational time and memory requirements.

To assess the accuracy and the efficiency of the TPT solution technique, comparisons are made to a direct numerical solution procedure with far-field radiation boundary conditions of arbitrary order developed by Hagstrom and Hariharan [21]. The direct numerical simulation code uses a second order central difference, however, boundary conditions are treated to the desired order accuracy. Hence it has no other a priori errors other than discretization errors. A 20th order boundary condition will be implemented in the DNS solutions shown herein.

On the physical boundary $r = 1$, the acoustic pressure is specified as

$$p(1, \theta, t) = \mathrm{e}^{-t}(1 - \cos t)\cos(m\theta). \tag{36}$$

Here m is modal number that indicates the dominant angular dependence on the boundary. In general this data could be represented by a general Fourier series with time-dependent coefficients. In the unbounded exterior domain, the convective wave equation is solved subject to an acoustic radiation condition.

It should be noted that even though the physical problem is posed exterior to a circle, the problem in the Laplace transform domain requires transformations to both the acoustic pressure and the spatial coordinates. In this process, the circular boundary maps to an ellipse (see Fig. 2), and as the Mach number increases, the eccentricity of the ellipse increases. The transformations are summarized by

$$\bar{p} = \tilde{p}\mathrm{e}^{-\lambda_{SX}}, \quad \bar{x} = \frac{x}{1-M^2}, \quad \bar{y} = \frac{y}{\sqrt{1-M^2}}.$$

These transformations map the boundary defined by the circle of radius 1 to the ellipse

$$\left(1-M^2\right)^2\bar{x}^2 + \left(1-M^2\right)\bar{y}^2 = 1.$$

Moreover, the polar representation of the boundary that is required by the integral equation procedure takes the form

$$r(\bar{\theta}) = \sqrt{\frac{1}{\left(1-M^2\right)^2\cos^2\bar{\theta} + \left(1-M^2\right)\sin^2\bar{\theta}}}.$$

From this $r'(\bar{\theta})$ and $r'\prime(\bar{\theta})$ are calculated for the various components of the assembly of the kernel of the integral equation.

Using the numerical Laplace transform techniques outlined above, the Laplace transform of the acoustic pressure on the boundary was determined in 13 s with the optimal value of $a_{\mathrm{opt}} = 0.0209$ for $N = 100$ and $T = 20$. Changing either N or T will yield a different value for a_{opt}.

8.1. Freestream Mach number $M = 0$

Our first result illustrates the propagation of acoustic waves in a domain $1 < r < 3$ for vanishing Mach number, that is $M = 0$. For this case, the convective wave equation reduces to a regular wave equation. TPT

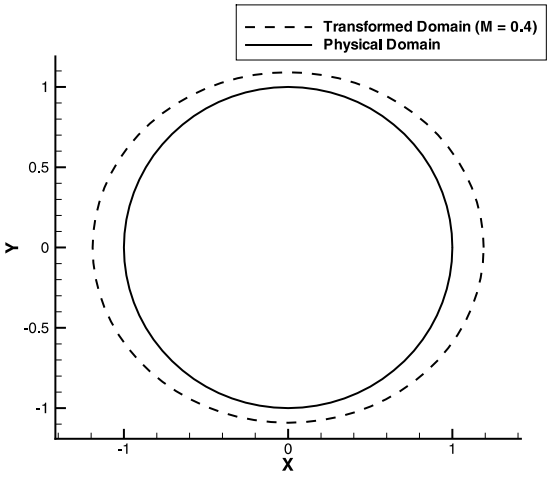

Fig. 2. Kirchhoff surface for the test problem $M = 0.4$.

solutions are shown in Fig. 3 at a location $(3,0)$ for $0 < t < 20$. The TPT solution is dependent on two parameters:

1. The number of points on the boundary n_θ for the discretization of the boundary integral, referred in the graph as the angular resolution.
2. The number of terms N in the inverse Laplace transform referred in the graph as the frequency resolution.

Fig. 3(a) shows the time history of the acoustic pressure at $(r,\theta) = (3,0)$ over $0 < t < 20$. At this scale, differences between the solutions are minimal. However, Fig. 3(b) shows a small portion of the time history where the differences between each solution are more apparent. Increasing the angular resolution n_θ or the frequency resolution N improved the solution at some expense in computational time. Little difference is seen between $n_\theta = 300$ and $n_\theta = 500$. Thus, the parameters $n_\theta = 300$ and $N = 100$ gave an acceptable solution with the minimum computational effort. These parameters are used for the remainder of the computations shown. Fig. 4 directly compares the most efficient TPT solution ($n_\theta = 300$ and $N = 100$) with the direct numerical simulation. In Fig. 5, contour plots compare the solutions at $\theta = 0$ and $\theta = \pi$ over $0 \leqslant r \leqslant 3$ is shown. As illustrated in the figures, agreement is evident.

The computational efficiency of the TPT method versus the direct numerical simulations is illustrated in Fig. 6. It should be noted that the solution domain for the direct numerical simulation was $1 < r < 3$. This was only possible due to the higher order boundary condition (order 20) within the code. If the solution is to be computed in a larger domain, the computational time and the required number of grid points for the direct simulation will be substantially increased from the current calculations. On the other hand, given the potential density the determination of the pressure at another location simply requires evaluation of Eq. (19) and the application of the inverse Laplace transform, given in Eq. (35). Therefore, as the size of the domain is increased the ratio of the timings between the TPT and the DNS will increase substantially.

8.2. Freestream Mach number $M = 0.4$

Our second result illustrates the propagation of the disturbance from $r = 1$ for Mach number $M = 0.4$ over the interval $0 < t < 20$ on an extended domain $1 < r < 10$. The increase in freestream Mach number and the size of the domain will both substantially increase the time required to calculate the direct numerical simulation, and the efficiency of the TPT technique will become more apparent. The forcing function $p(1,\theta,t)$ remains identical to the $M = 0$ case considered above. The direct simulation was per-

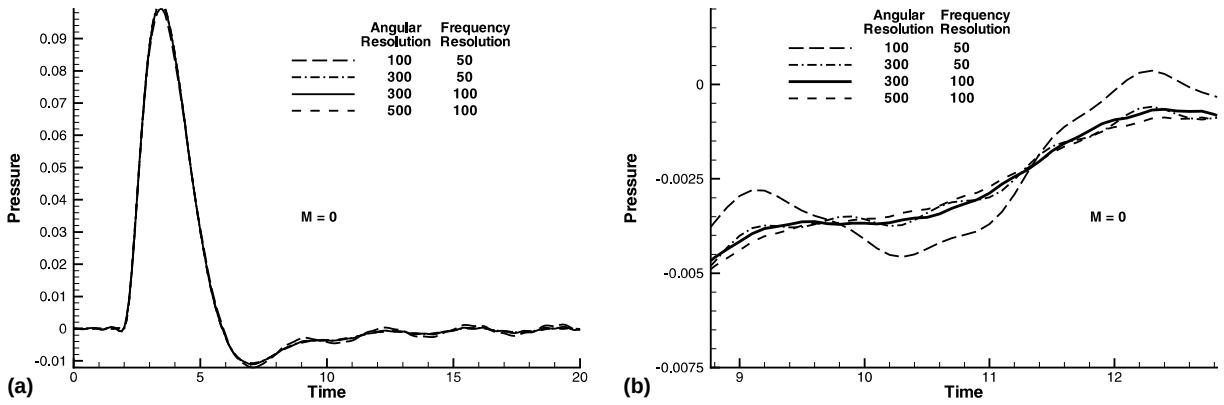

Fig. 3. Time history of the acoustic response for $M = 0$ at $(3,0)$. (a) Acoustic response over the entire interval $0 < t < 20$. (b) Detail of the acoustic response.

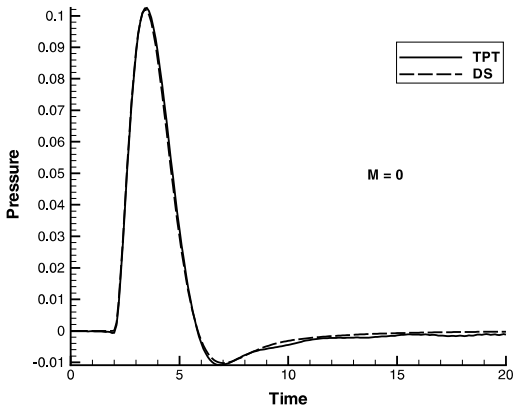

Fig. 4. Comparison of TPT with direct numerical simulation for $M = 0$.

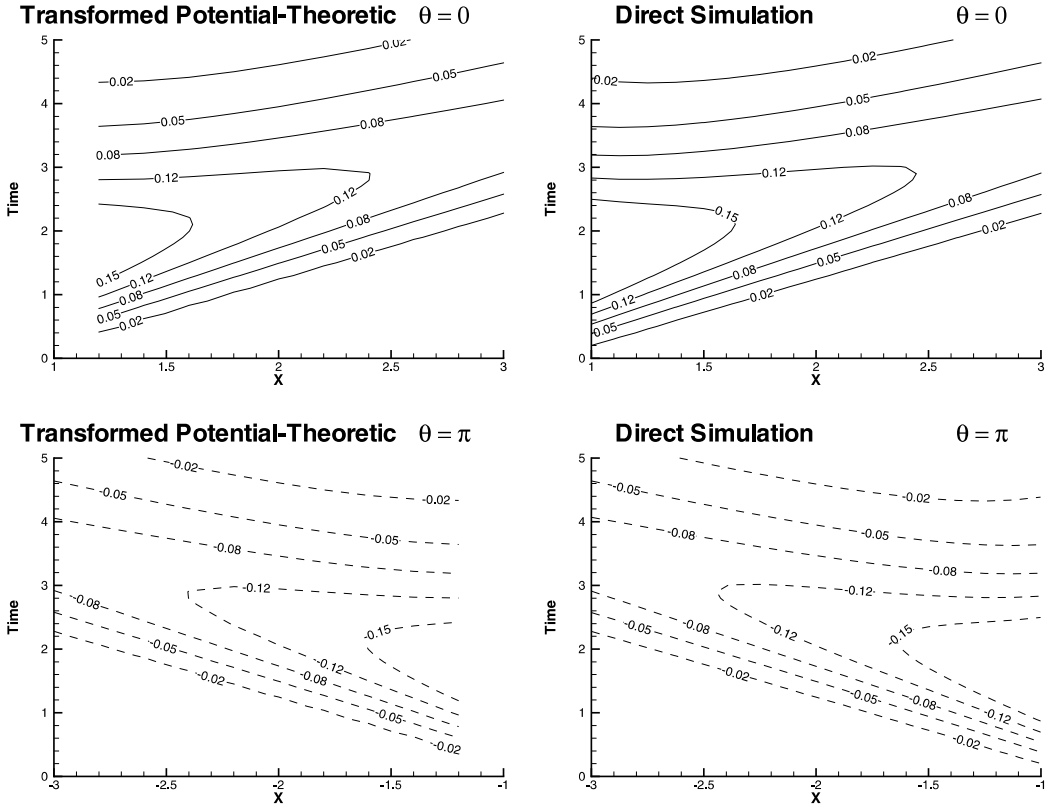

Fig. 5. Comparison of contours between the TPT and DNS for $M = 0$.

formed in the annular domain $1 < r < 10$ using 20th-order far-field boundary conditions and a grid size increased to 2700×201 to maintain resolution. The accuracy of the TPT technique is independent of the size of the domain, so $n_\theta = 300$ points on the interior boundary and $N = 100$ terms in the inverse Laplace transform with $a_{\text{opt}} = 0.0209$ were used.

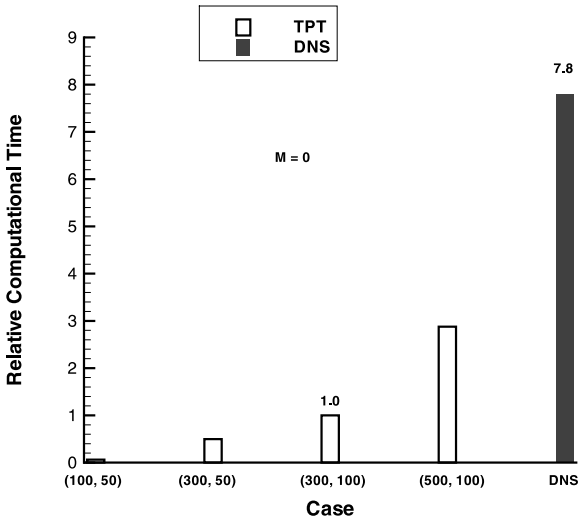

Fig. 6. Computational efficiency: $M = 0$, $1 < r < 3$.

The pressure on the boundary is transformed into the Laplace domain and used to determine the double layer potential density. Fig. 7 shows the real and imaginary parts of the double layer potential density as a function of the frequency and angular position. The double layer potential density is then used to determine the far-field frequency domain pressure, as seen in Fig. 8. Finally, the far-field pressure is transformed back into the time domain, shown in Fig. 9. Recall that the TPT technique is meshless and the pressure need only be calculated at the point or points of interest.

Time slices show the wave propagation in the annulus of computation in Fig. 10. Note that the propagation speeds are retarded in the upstream direction ($1 - M = 0.6$) and accelerated ($1 + M = 1.4$) in the downstream direction. Finally, pressure contours for the $M = 0.40$ large domain case $1 < r < 10$ are shown in Figs. 11(a) and (b), where the contours are plotted on a grid with 54 points along the x-axis. Excellent agreement is again seen between the methods.

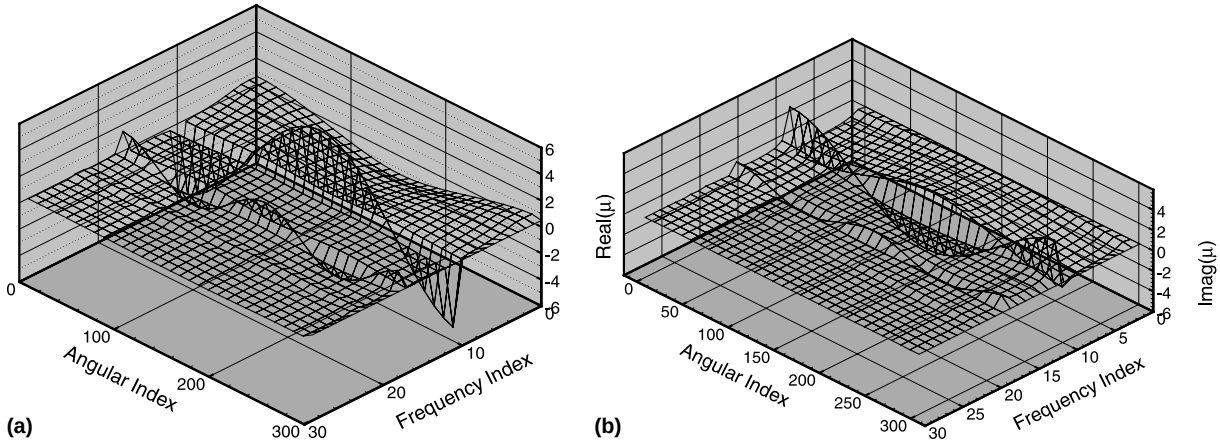

Fig. 7. Double layer potential density with $M = 0.4$. (a) Real part of the double layer potential density μ. (b) Imaginary part of the double layer potential density μ.

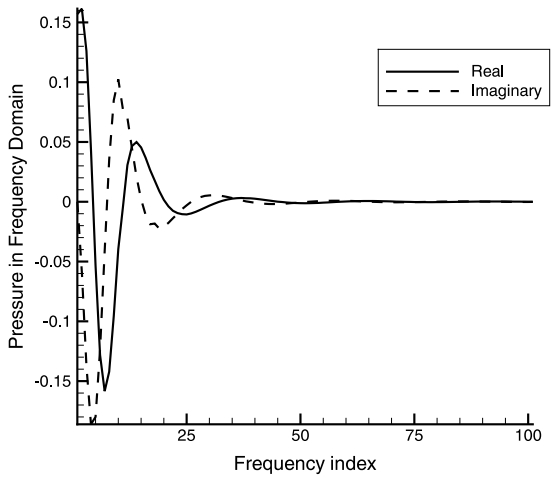

Fig. 8. Far-field acoustic pressure in the frequency domain $M = 0.4$ at $\theta = 0$ and $r = 3$.

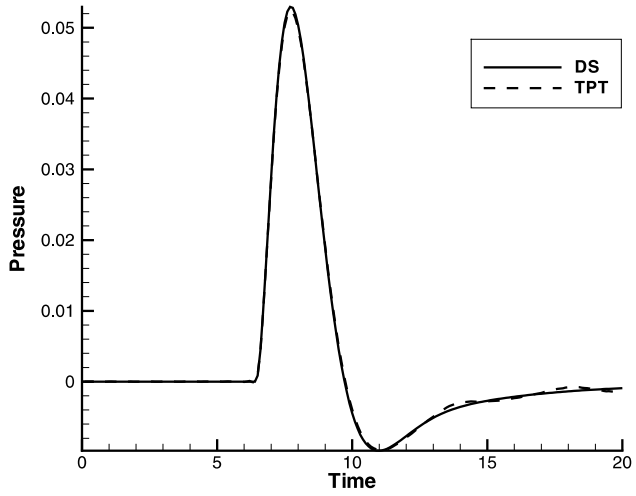

Fig. 9. Acoustic response with $M = 0.40$. The time history of the pressure response is shown at $(r, \theta) = (10, 0)$.

The computational efficiency of the TPT technique is summarized in Fig. 12. Direct simulation over the entire annular domain $1 < r < 10$ required 313 min. The TPT method required 1.1 and 1.3 min to generate the solutions shown in Figs. 9 and 11(a), respectively.

9. Discussion and conclusions

The transform/potential theoretic (TPT) technique has been developed for calculating far-field sound propagation into an acoustic medium from time-dependent pressure on a Kirchhoff surface in the presence of mean flow. In particular, double layer potential theory in combination with Laplace transform techniques are used to develop a semi-analytical method which is computationally efficient and moreover has

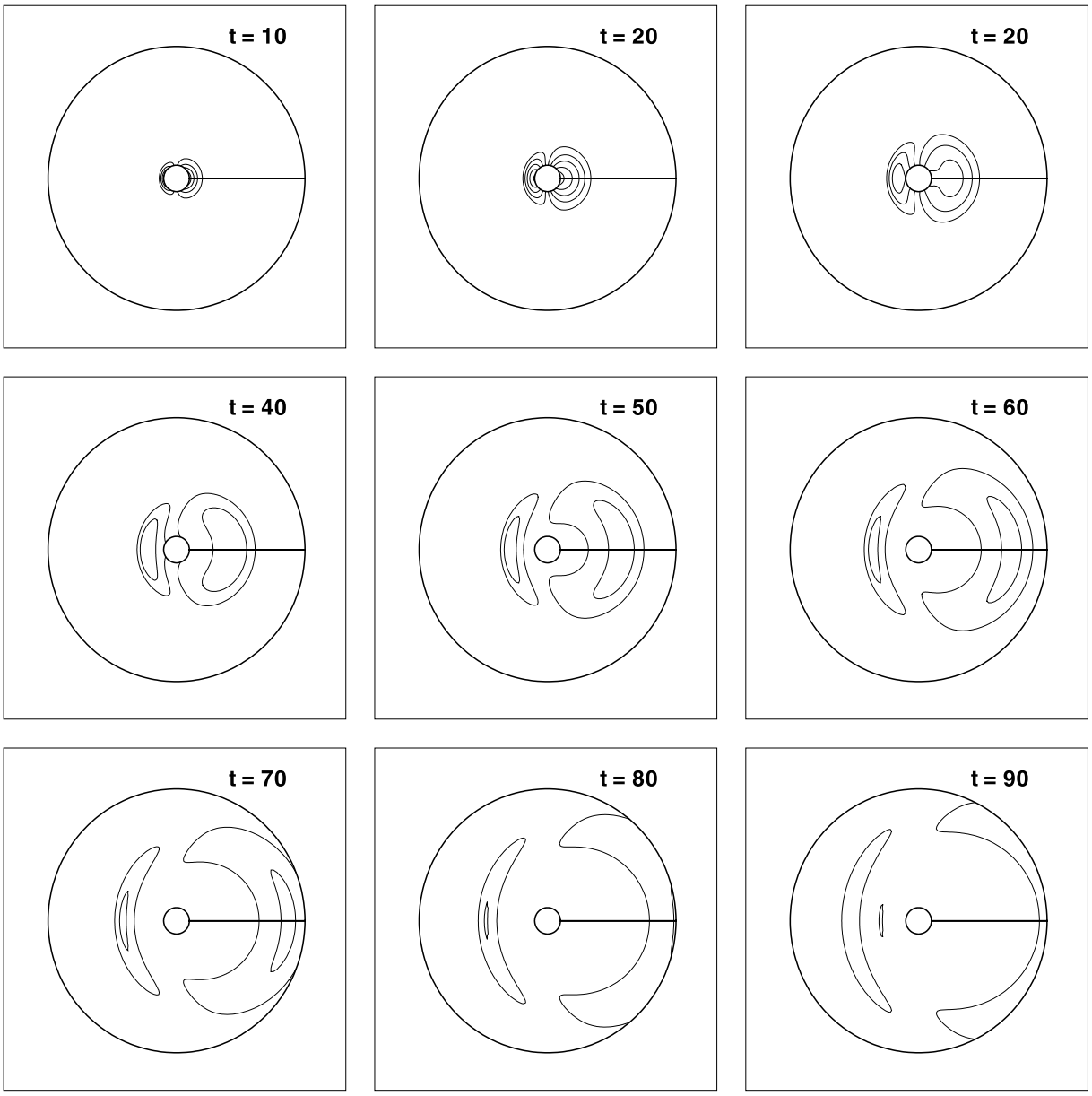

Fig. 10. Wave propagation in the annulus of computation: $M = 0.40$.

exact far-field radiation conditions built in to the formulation. As illustrated in the two-dimensional test problems, this method leads to solutions which compare well with existing results, while requiring computational resources several orders of magnitude below direct simulations.

As presented in this paper, this technique is restricted to the solution of linear acoustics with uniform mean flow. However, one can imagine a perturbative approach in which this technique is used for the solution of variational problems at increasing order of approximation for more complicated problems. In addition, one can pursue the extension of this method to three-dimensional acoustic problems.

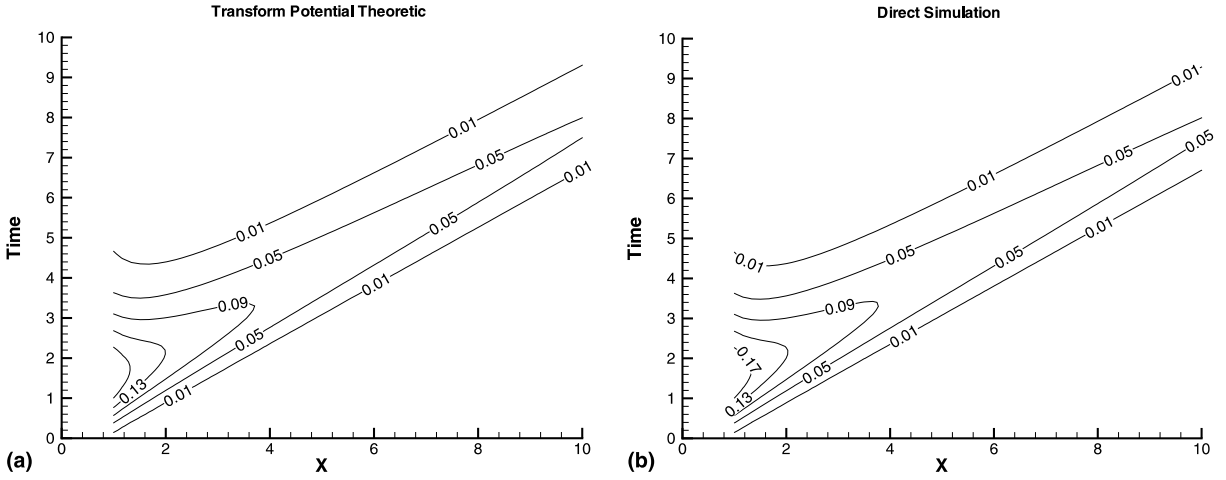

Fig. 11. TPT and DNS contours for $M = 0.4$ along $1 < x < 10$.

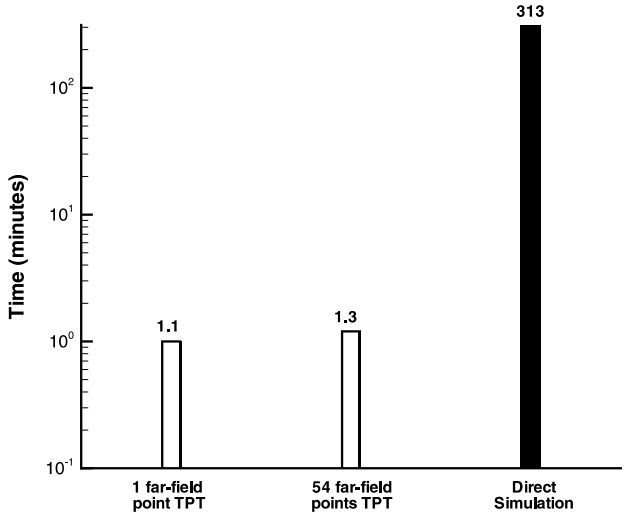

Fig. 12. Computational efficiency: $M = 0.4$, $1 < r < 10$.

References

[1] H.M. Atassi, Unsteady Aerodynamics of vortical flows: early and recent developments, Symposium on Aerodynamics and Aeroacoustics, Feb. 28–March 2, 1993.
[2] H.M. Atassi, S. Subramaniam, J.R. Scott, Acoustic radiation from lifting airfoils in compressible subsonic flows, AIAA Paper 90-3911, October, 1990.
[3] H.M. Atassi, M. Dusey, C.M. Davis, Acoustic radiation from a thin airfoil in non-uniform subsonic flows, AIAA Paper 90-3910, October, 1990.
[4] S.I. Hariharan, R.C. MacCamy, Integral equation procedures for eddy current problems, J. Comput. Phys. 45 (1) (1982) 80–99.
[5] S.M. Patrick, C.M. Davis, H.M. Atassi, Acoustic Radiation from a Lifting Airfoil in Nonuniform Subsonic Flows, FED-Vol. 147, Computational Aero- and Hydro-Acoustics, ASME, 1993.
[6] S.M. Patrick, The acoustic directivity from airfoils in nonuniform subsonic flows, M.S. Dissertation, University of Notre Dame, Notre Dame, IN, 1993 (unpublished).

[7] J.R. Scott, Compressible flows with periodic vortical disturbances around lifting airfoils, Ph.D. Dissertation, University of Notre Dame, IN, May, 1990 (unpublished).
[8] J.R. Scott, H.M. Atassi, A finite-difference, frequency-domain numerical scheme for the solution of the gust response problem, J. Comput. Phys. 119 (1995) 75–93.
[9] C.L. Bennett, W.L. Weeks, Transient scattering from conducting cylinders, IEEE Trans. AP (9) (1970) 627–633.
[10] B. Davies, B. Martin, Numerical inversion of the laplace transform: a survey and comparison of methods, J. Compt. Phys. 33 (1979) 1–32.
[11] W. Weeks, Numerical inversion of Laplace transforms using Laguerre functions, J. ACM 13 (3) (1966) 419–426.
[12] R. Piessens, M. Branders, Numerical inversion of the Laplace transform using generalized Laguerre polynomials, Proc. IEEE 118 (10) (1971) 1517–1522.
[13] J.N. Lyness, G. Giunta, A modification of the weeks method for numerical inversion of the Laplace transform, Math. Comput. 47 (175) (1986) 313–322.
[14] B. Gabutti, P. Lepora, The numerical performance of Tricomi's formula for inverting the laplace transform, Numer. Math. 51 (1987) 369–380.
[15] H. Dubner, J. Abate, Numerical inversion of laplace transforms by relating them to the finite fourier cosine transform, J. ACM 15 (1) (1968) 115–123.
[16] G. Honig, U. Hirdes, Algorithm 27: A method for the numerical inversion of laplace transforms, J. Comput. Appl. Math. 10 (1984) 113–132.
[17] H.T. Chen, T.M. Chen, C.K. Chen, Hybrid Laplace transform/finite element method for one-dimensional transient heat conduction problems, Comput. Methods Appl. Mech. Engrg. 63 (1987) 83–95.
[18] S.I. Hariharan, Ed. Stenger, J.R. Scott, Potential theoretic methods for far field sound radiation calculations, ICOMP Report-95-26, NASA Technical Memorandum 107118, 1995.
[19] S.I. Hariharan, K. Kreider, J.R. Scott, A potential theoretic method for far field sound radiation, J. Comput. Phys. 164 (2000) 143–164.
[20] T. Hagstrom, S.I. Hariharan, A formulation of asymptotic and exact boundary conditions using local operators, Appl. Numer. Math. 27 (1998) 397–401.
[21] T. Hagstrom, S.I. Hariharan, High-order radiation boundary conditions for the convective wave equation in exterior domains, SIAM J. Sci. Comput. (submitted).
[22] M. Abramowitz, I. Stegun, Handbook of Mathematical Functions, Dover, New York, 1970.
[23] L. Thompson, R. Huan, Computation of far-field solutions based on exact nonreflecting conditions for the time-dependent wave equation, Comput. Methods Appl. Mech. Engrg. 190 (2000) 1551–1577.
[24] L. Thompson, P. Pinsky, A space–time finite element method for structural acoustics in infinite domains. Part 2: Exact time-dependent non-reflecting boundary conditions, Comput. Methods Appl. Mech. Engrg. 132 (1996) 229–258.
[25] L. Thompson, R. Huan, Implementation of exact nonreflecting boundary conditions in the finite element method for the time-dependent wave equation, Comput. Methods Appl. Mech. Engrg. 187 (2000) 137–159.
[26] B. Alpert, L. Greengard, T. Hagstrom, An integral evolution formula for the wave equation, J. Comput. Phys. 162 (2000) 536–543.
[27] B. Alpert, L. Greengard, T. Hagstrom, Rapid evaluation of nonreflecting boundary kernels for time-domain wave propagation, SIAM J. Numer. Anal. 37 (2000) 1138–1164.
[28] A.S. Lyrintzis, Review: the use of Kirchhoff's method in computational aeroacoustics, J. Fluids Eng. (1994) 665–676.